# Nanoscale

Accepted Manuscript


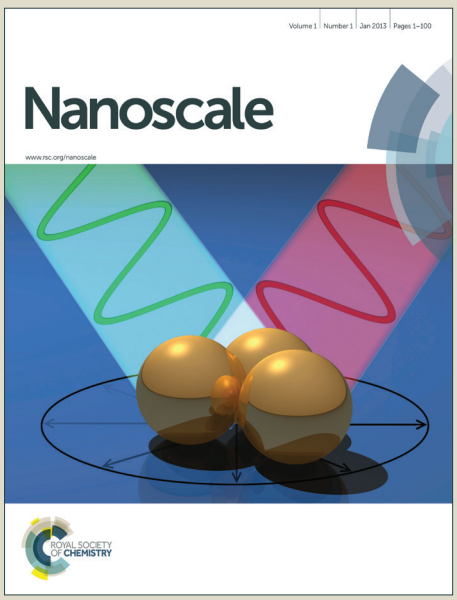





ROYAL SOCIETY OF CHEMISTRY

www.rsc.org/nanoscale

Journal Name

Nanoscale

Dynamic Article Links ►

Cite this: DOI: 10.1039/c0xx00000x

www.rsc.org/xxxxxx

ARTICLE TYPE

# The mechanically tough, elastic and stable rope-like double nanohelices

**L. Dai,*[a] X. J. Huang,[b] L. X. Dong,[c] Q. Zhang,[d] and L. Zhang, *[d]**

***Received (in XXX, XXX) Xth XXXXXXXXX 20XX, Accepted Xth XXXXXXXXX 20XX***
**DOI: 10.1039/b000000x**

Double helix nanostructures have been the object of intense theoretical and experimental investigations in recent years due to their various kinds of available materials and unique morphology. Among these structures, rope-like double nanohelices of two strands contacting along a line can be obtained by any one-dimensional nanostructures. In this work, we establish a novel theory for quantitatively exploring statics and dynamics of the rope-like double nanohelices by employing the concept of the extensible Cosserat curve. The rope-like double nanohelices are tough, relatively elastic, and mechanically stable, which agrees well with the experiments. The characteristics of the interaction between two strands, tensile modulus and torque are precisely described and explained in the entire stretching region. The proposed model offers deep quantitative insight in the mechanics of the double helix nanostructures, and supplies a reliable reference for further experimental research.

## 1. Introduction

Helices are ubiquitous in plantae, bacteria, fungi, metazoa and artificial materials, such as tendrils, vines, bacterial shape in spirochetes, aerial hyphae in actynomycetes, horns, $\alpha$-helices, self-rolled nanosprings and carbon nanotubes.[1-11] Two spiral and spatially arranged strands form a double helix, which therefore has not only the advantages of single helices: e.g. superelasticity [12-14] and piezoresistive, piezoelectric effects,[15-17] but also the benefits that the interaction between strands brings. Except for the double helix structures in nature, e.g. the most famous DNA (Fig 1(a)),[18] scientists also made many synthetic efforts to mimic this fascinating morphology because of their unique shapes and the corresponding applications in various areas.[19,20] In 1990 double helix was firstly obtained from carbon nanofibers, and it was found that the coiled filaments could be extended elastically up to about three times versus the original coil length and had no permanent deformation after loading.[21,22] In recent years, further research on such double helix carbon nanofibers as well as other nanomaterials were still carried on, shown in Table 1, and these double nanohelices provide excellent strength, stability and conductivity.[23-27]

Among all the double nanohelices, there is one type that two strands of elastic wires wind around each other while contacting along a line, resembling a rope. Such double nanohelices can be obtained by the following approaches as shown in Table 1. The rope-like carbon double nanohelices were synthesized by pyrolysis of acetone using iron nanoparticles as catalysts;[28] the Au-Ag alloy nanowires got twisted when a metal layer of Pd, Pt, or Au was deposited on them (Fig. 1(b));[29] the double helix microtubes of silicon were formed by using a Zintl compound NaSi as the starting material (Fig. 1(c));[30] an overtwisted single carbon nanowire released around itself until it reached a torque-balanced state (Fig. 1(d)).[31] Remarkably, the fourth method could be applied to diverse nanowires, nanotubes and nanorods which significantly increase the posibility for the controllable formation of double nanohelices. Moreover, it was reported that in contrast with the singles yarn of carbon, the two-ply yarn had higher tensile strengths between 250 and 460 MPa, and higher breaking work of 20 J/g.[31] Though the physical properties of the double helix Si microtubes and (Au-Ag)@Pd nanowires are yet to be fully explored, some experimental results indicated that the rope-like double nanohelices have excellent mechanical properties for serving as building blocks in MEMS/NEMS. Thus, for the rope-like double nanohelices, an accurate theoretical description of the elasticity behaviour is necessary, and yet to be constructed.

Since the elongation of an axial loaded rope-like double nanohelix completely comes from the stretch of two strands, the elastic deformation of the material must not be neglected. In this paper, we shed light on the elastic properties of the double nanohelices by considering a Cosserat curve with four kinds of deformation, i.e., bending, torsion, extension and shear. We can obtain a set of expressions that allow us to quantitatively measure the mechanical properties of the double helix system, such as the interaction between the strands, tensile modulus and torque. Also, it is revealed that when nanowires/nanotubes wind into double helix structures, the structure becomes mechanically stronger, more reversibly deformable over relatively large strains to absorb energy and maintain the linear elasticity. This approach provides a framework to study both statics and dynamics of the double nanohelices.

## 2. Results and Discussion

The Cosserat curve, as an elastic directed one, is appropriately used to study the statics and the dynamics of continuous rods with extensibility and shear deformation.[32] When a double

nanohelix with a straight contact line between two strands is loaded by a force along its helical axis, the elongation of the double nanohelix is totally resulted from the stretch of the strands. To describe the elasticity of double nanohelices precisely, we regard the strands as Cosserat curves. The basic equilibrium equations of each strand can be written as:[33]

$$\hat{\tau}_\alpha - \varepsilon_{\alpha\beta\gamma}\tau_\beta W_\gamma + f_\alpha = 0\,, \tag{1a}$$

$$\hat{m}_\alpha - \varepsilon_{\alpha\beta\gamma}\left(m_\beta W_\gamma + \tau_\beta y_\gamma\right) = 0\,, \tag{1b}$$

where $\tau$ and $m$ are the total force and torque across the cross section of the curve, respectively, $\varepsilon$ is the permutation tensor, and $W$ and $y$ are the director and position deformation measure, respectively. $f$ is the distributed forces per unit length, *i.e.*, the interaction between two strands. The Greek subscripts $\alpha$, $\beta$, $\gamma$ take on the values 1, 2, 3. and is the stretch of the curve with $S$ the arc length along a fixed reference configuration and $s$ the one along a deformed configuration.

As shown in Fig. 2(a)-(c), to explore the mechanical properties of rope-like double nanohelices, we suppose that under a constant torque $M$ two straight nanowires with circle cross section of radius $r_0$, length $L_0$ twist around each other to form an uniform free standing double helix $H_{\mathrm{DI}}$, with the coil wire radius $r_1$, radius $a_1 = r_1$,[34] pitch $b_1$, helix angle $\zeta = \arctan(2\pi r_1/b_1)$, and the helix axis, *i.e.* the straight contact line between the two strands, along the direction of $M$. There are several methods to provide the torque $M$: e.g. metal deposition on nanowires[29] and overtwisting a single yarn[31]. In particular, for a double helix consisting of two free standing single helices, its two strands maintain the helix structures after separation and there is no torque applied on it, *i.e.*, $M$=0. The carbon double nanohelix synthesized by catalytic pyrolysis of acetone is such a case.[28] The area of the $H_{\mathrm{DI}}$ transection is $A=2\pi r_1^2/\cos\zeta$.When $H_{\mathrm{DI}}$ is loaded under a force $F$ along its helix axis, it transforms to the elongated double helix $H_{\mathrm{DF}}$ of the coil wire radius $r_2$, radius $a_2 = r_2$, and pitch $b_2$. Fig. 2(a')-(c') presents the partial enlargement of the straight nanowires, as well as the corresponding one of $H_{\mathrm{DI}}$ and $H_{\mathrm{DF}}$ with the stretching length $\Delta L$ of nanowire. In this model, the above situation can be simplified that two initially straight nanowires with circle cross section of radius $r_0$, length $L_0$ bent into a double helix form $H_{\mathrm{D}}$ ($H_{\mathrm{DI}}$ or $H_{\mathrm{DF}}$) of the coil wire radius $r$, radius $a = r$, pitch $b$ and they are held in equilibrium by a force $F$ and a moment $M$ at the ends of the nanowires. The straight nanowires structure is the fixed reference configuration and $H_{\mathrm{D}}$ is the deformed one.

As shown in Fig. 2(a')-(c') $\boldsymbol{D}_i$ (i=1,2,3) and $\boldsymbol{d}_i$ (i=1,2,3) are the director basis of one strand of the straight nanowires and $H_{\mathrm{D}}$, respectively. We choose the first director $\boldsymbol{d}_1$ and the second director $\boldsymbol{d}_2$ along the direction of the largest and smallest bending stiffness of the cross section in $H_{\mathrm{D}}$, and the helix axis along the $\boldsymbol{e}_3$ axis of the fixed Cartesian basis. For such a case the director deformation measures $W^{(0)}$ of the straight nanowires and $W$ of $H_{\mathrm{D}}$ have the form of:

$$W_1^{(0)} = 0\,,\ W_2^{(0)} = 0\,,\ W_3^{(0)} = \dot{\psi}_0\,, \tag{2a}$$

$$W_1 = 0\,,\ W_2 = \hat{\psi}\sin\theta\,,\ W_3 = \hat{\psi}\cos\theta\,. \tag{2b}$$

where $\theta_0$, and $\theta$, are the Euler angles used to define $\boldsymbol{D}_i$ and $\boldsymbol{d}_i$, respectively.[35] For the configuration of helix $\theta_0$,, $\theta$, are all constants,[36] and .[37] Under the assumption of the third director $\boldsymbol{D}_3$ along the tangent to the centerline of the straight nanowire, the force and torque in equation (1) yield:

$$\tau_1 = E_1 y_1\,,\ \tau_2 = E_2 y_2\,,\ \tau_3 = E_3(y_3 - 1)\,, \tag{3a}$$

$$m_1 = A(W_1 - W_1^{(0)})\,,\ m_2 = B(W_2 - W_2^{(0)})\,,\ m_3 = C(W_3 - W_3^{(0)})\,, \tag{3b}$$

where ,and . $K_2$ is the Timoshenko shear coefficients and related to the Poisson's ratio $v$ through .[38] $E$ and $G$ are the Young's and shear moduli, respectively. $I=(\pi r_0^4)/4$ is the moment of inertia and $J=(\pi r_0^4)/2$ is the polar moment of inertia of the cross section. We use Eq. (3) in the equilibrium equation Eq. (1b) and obtain:

$$B(\hat{W}_1 - \hat{W}_1^{(0)}) - (B-C)W_2W_3 + BW_2^{(0)}W_3 - CW_3^{(0)}W_2 - (E_2 - E_3)y_2y_3 - E_3y_2 = 0\,, \tag{4a}$$

$$B(\hat{W}_2 - \hat{W}_2^{(0)}) + (B-C)W_1W_3 - BW_1^{(0)}W_3 + CW_3^{(0)}W_1 + (E_2 - E_3)y_1y_3 + E_3y_1 = 0\,, \tag{4b}$$

From Eqs. (2), (3a), (4b) and $\hat{W}^0 = \hat{W} = 0$ we have:

$$y_1 = 0\,,\ \tau_1 = 0 \tag{5}$$

According to Eqs. (2) to (4), $\tau$ is the function of and $\theta$, which leads to:

$$\hat{\tau}_i = 0\,,\ (i=1,2,3)\,. \tag{6}$$

The equilibrium equation Eq. (1a) yields:

$$\hat{\tau}_1 - \tau_2W_3 + \tau_3W_2 = -f_1\,, \tag{7a}$$

$$\tau_1W_3 + \hat{\tau}_2 - \tau_3W_1 = -f_2\,, \tag{7b}$$

$$-\tau_1W_2 + \tau_2W_1 + \hat{\tau}_3 = -f_3\,, \tag{7c}$$

Combining Eqs. (2b), (5), (6) with Eqs. (7b), (7c), we obtain:

$$f_2 = f_3 = 0\,,\ \boldsymbol{f} = f_1\boldsymbol{d}_1\,. \tag{8}$$

Since $\boldsymbol{d}_1 \perp \boldsymbol{e}_3$, Eq. (8) shows that the interaction $\boldsymbol{f}$, marked by the red arrows in Figs. 2(b') and 2(c'), lies in the plane perpendicular to the $\boldsymbol{e}_3$ axis, *i.e.* the helix axis of the double helix, which is consistent with the conclusion given by Neukirch.[39] It follows from Eqs. (2b), (6) and (7a) that

$$-\tau_2\hat{\psi}\cos\theta + \tau_3\hat{\psi}\sin\theta = -f_1\,. \tag{9}$$

Considering that the loading force $F$ is along the helix axis of the double helix, we find that the axial force balance for each nanowire gives $F'=F/2$ and

$$\boldsymbol{\tau}\bullet\boldsymbol{e}_3 = F'\,. \tag{10}$$

Inserting Eq. (2) into Eq. (10) gives the following relationship:

$$\tau_2\sin\theta + \tau_3\cos\theta = F'\,. \tag{11}$$

By virtue of Eqs. (9) and (11), the total force across the cross

section of the curve can be expressed as:

$$\tau_2 = F'\sin\theta + \frac{f_1}{\hat{\psi}}\cos\theta,\ \tau_3 = F'\cos\theta - \frac{f_1}{\hat{\psi}}\sin\theta. \quad (12)$$

Then the Eqs. (3a), (5) and (12) give the position vectors of $H_D$:

$$y_1 = 0,$$

$$y_2 = \frac{F'}{E_2}\sin\theta + \frac{f_1}{\hat{\psi}}\frac{1}{E_2}\cos\theta,\ y_3 = \frac{F'}{E_3}\cos\theta - \frac{f_1}{\hat{\psi}}\frac{1}{E_3}\sin\theta + 1. \quad (13)$$

From Eq. (13), we can have not only the stretch $\lambda$:

$$\lambda = \sqrt{\left(\frac{F'}{E_2}\sin\theta + \frac{f_1}{\hat{\psi}}\frac{1}{E_2}\cos\theta\right)^2 + \left(\frac{F'}{E_3}\cos\theta - \frac{f_1}{\hat{\psi}}\frac{1}{E_3}\sin\theta + 1\right)^2}, \quad (14)$$

but also the radius and pitch of $H_D$ in terms of the Euler angles:

$$r = a = \frac{1}{\hat{\psi}}\left[\left(\frac{F'}{E_2}\sin\theta + \frac{f_1}{\hat{\psi}}\frac{1}{E_2}\cos\theta\right)(-\cos\theta) + \left(\frac{F'}{E_3}\cos\theta - \frac{f_1}{\hat{\psi}}\frac{1}{E_3}\sin\theta + 1\right)\sin\theta\right], \quad (15a)$$

$$b = \frac{2\pi}{\hat{\psi}}\left[\left(\frac{F'}{E_2}\sin\theta + \frac{f_1}{\hat{\psi}}\frac{1}{E_2}\cos\theta\right)\sin\theta + \left(\frac{F'}{E_3}\cos\theta - \frac{f_1}{\hat{\psi}}\frac{1}{E_3}\sin\theta + 1\right)\cos\theta\right]. \quad (15b)$$

Using Eqs. (2), (13) and , Eq. (4a) can be rewritten as:

$$\left(\frac{1}{E_3} - \frac{1}{E_2}\right)\sin\theta\cos\theta F'^2 + \left[\sin\theta + \left(\frac{1}{E_3} - \frac{1}{E_2}\right)\left(\cos^2\theta - \sin^2\theta\right)\frac{f_1}{\hat{\psi}}\right]F' + B\hat{\psi}^2\sin\theta\cos\theta - C\hat{\psi}^2\sin\theta\left(\cos\theta - 1\right) - \left(\frac{1}{E_3} - \frac{1}{E_2}\right)\sin\theta\cos\theta\left(\frac{f_1}{\hat{\psi}}\right)^2 + \cos\theta\frac{f_1}{\hat{\psi}} = 0 \quad (16)$$

Furthermore, the torque $M$ along the helix axis of the double helix is expressed by:

$$M = 2\left[B\hat{\psi}\sin^2\theta + C\hat{\psi}\left(\cos\theta - 1\right)\cos\theta\right]. \quad (17)$$

Due to the conservation of nanowire volume for the elastic deformation, the change of nanowire radius is rather small by comparison with the stretching length $\Delta L$ of nanowire. In order to simplify the analysis of the spring constant $h$ of $H_D$, we suppose that the radius of nanowire is maintained constant during the loading. Thus according to the Hooke's law $h=dF/d(Nb)$ it can be deduced from Eqs. (15) and (16) that

$$h = \frac{2}{N}\frac{P_1P_6 - P_3P_4}{P_1P_6P_8 + P_2P_4P_9 + P_3P_5P_7 - P_1P_5P_9 - P_2P_6P_7 - P_3P_4P_8},$$

where

$$P_1 \equiv \left(\frac{1}{E_3} - \frac{1}{E_2}\right)\left(\sin\theta - \frac{\cos^2\theta}{\sin\theta}\right)F'^2 - \frac{\cos\theta}{\sin\theta}F' + 4\frac{f_1}{\hat{\psi}}\left(\frac{1}{E_3} - \frac{1}{E_2}\right)\cos\theta F' + \left(B - C\right)\hat{\psi}^2\left(\sin\theta - \frac{\cos^2\theta}{\sin\theta}\right) - C\hat{\psi}^2\frac{\cos\theta}{\sin\theta} - \left(\frac{f_1}{\hat{\psi}}\right)^2\left(\frac{1}{E_3} - \frac{1}{E_2}\right)\left(\sin\theta - \frac{\cos^2\theta}{\sin\theta}\right) + \frac{f_1}{\hat{\psi}}$$

$$P_2 \equiv 2\left(\frac{1}{E_3} - \frac{1}{E_2}\right)\sin\theta\cos\theta F' + \sin\theta + \frac{f_1}{\hat{\psi}}\left(\frac{1}{E_3} - \frac{1}{E_2}\right)\left(2\cos^2\theta - 1\right)$$

$$P_3 \equiv \frac{1}{\hat{\psi}}\left(\frac{1}{E_3} - \frac{1}{E_2}\right)\left(2\cos^2\theta - 1\right)F' - 2\frac{f_1}{\hat{\psi}^2}\left(\frac{1}{E_3} - \frac{1}{E_2}\right)\sin\theta\cos\theta + \frac{\cos\theta}{\hat{\psi}}$$

$$P_4 \equiv \left(\frac{1}{E_3} - \frac{1}{E_2}\right)\left(\sin\theta - \frac{\cos^2\theta}{\sin\theta}\right)F' + 2\frac{f_1}{\hat{\psi}}\left(\frac{1}{E_3} - \frac{1}{E_2}\right)\cos\theta - \frac{\cos\theta}{\sin\theta}$$

$$P_5 \equiv \left(\frac{1}{E_3} - \frac{1}{E_2}\right)\sin\theta\cos\theta$$

$$P_6 \equiv \frac{1}{\hat{\psi}}\left(\frac{1}{E_3} - \frac{1}{E_2}\right)\cos^2\theta - \frac{1}{\hat{\psi}}\frac{1}{E_3}$$

$$P_7 \equiv \left[2\left(\frac{1}{E_3} - \frac{1}{E_2}\right)\cos\theta F' - \frac{f_1}{\hat{\psi}}\left(\frac{1}{E_3} - \frac{1}{E_2}\right)\left(\sin\theta - \frac{\cos^2\theta}{\sin\theta}\right) + 1\right]\frac{2\pi}{\hat{\psi}}$$

$$P_8 \equiv \left[\frac{1}{E_2} + \left(\frac{1}{E_3} - \frac{1}{E_2}\right)\cos^2\theta\right]\frac{2\pi}{\hat{\psi}}$$

$$P_9 \equiv \left[-\frac{1}{\hat{\psi}}\left(\frac{1}{E_3} - \frac{1}{E_2}\right)\sin\theta\cos\theta\right]\frac{2\pi}{\hat{\psi}}, \quad (18)$$

where $N$ is the number of the coils. If the nanowire has infinite resistance to shear and extension, *i.e.* $E_{2,3}\rightarrow\infty$, then $h\rightarrow\infty$ can be calculated from Eq. (18), which is consistent with the fact that the spring constant of a double helix made of inextensible wires is infinity.

By measuring the geometry parameters $r_1$, $b_1$ of the self-wind double helix $H_{DI}$ and the loading force $F$, we can obtain the radius $r_2$, the pitch $b_2$, the interaction $f$ between two strands, the stretch $\lambda$, the spring constant $h$ of the elongated double helix $H_{DF}$ as well as the torque $M$ along the helix axis through Eqs. (14-18) with the conservation of the nanowire length and that of the nanowire volume, or just with the approximation of $r_0=r_1=r_2$ used in the calculation of the spring constant $h$.

This paper will use the (Au-Ag)@Pd double nanohelices[29] as an example to quantitatively analyze the mechanical performance of rope-like double nanohelices with the aid of the proposed Cosserat curve model. Upon growth of an additional metal layer Pd, two Au-Ag alloy NWs wind around themselves to form a free standing double helix $H_{DI}$ with geometry parameters of $r_1$=3.5nm, $b_1$=47nm,[29] and helix angle $\zeta$=25 º. Supposing that Au, Ag and Pd are weighted equally and contribute the same percentage of the material, we can get the torque , interaction force per unit length from Eqs. (15-17) with , $b = b_1$, $F = 0$ as well as the average material parameters of $E$=98GPa, $\upsilon$=0.38 ($E_{Au}$=70GPa,[39] $E_{Ag}$=102GPa,[40] $E_{Pd}$=121GPa, $\upsilon_{Au}$=0.43,[41] $\upsilon_{Ag}$=0.31,[42] $\upsilon_{Pd}$=0.39.[43]). Since the theoretical value of ultimate tensile strengths (UTS) is

$E$/10 for small-diameter nanowires,[44] the UTS of the (Au-Ag)@Pd double nanohelices is 9.8GPa. With the UTS, Fig. 3(a) shows the tensile stress $F/A$ versus the tensile strain $(b_2-b_1)/b_1$ of the elongated double nanohelix $H_{DF}$ in the entire stretching processes for not only $\zeta$=25 º, but also the $\zeta$ differing by ±10 ºfrom 25 ºand the boundary values of 45 ºand 0 º(two parallel straight lines).[34] The modeling results are deduced from Eqs. (15-16) with $r = r_2$ , $b = b_2$, the average material parameters and the corresponding geometry parameters of the double nanohelices of five different helix angles. All the stress-strain curves remain linear during the loading, which is consistent with the experimental results of the carbon double nanohelix in the low-strain region, as the material deformation can be considered as elastic.[31] It is found that the maximum tensile strain increases from 3.2% to 27.0% with increasing the helix angle $\zeta$ from 0 ºto 45 º. Compared to the straight wires, the double helix structures are more deformable over relatively large strains to absorb energy. Furthermore if two straight wires wind into a double helix of , the maximum load $F_{max} = A$•UTS of the material will be raised by a factor of 1.4.

Finite element method (FEM) simulations (Autodesk Simulation Mechanical) are also applied to estimate the displacements of the double helix under ten discrete load forces within the UTS range. Since the minimum input value is 1000nm, a micronscale double helix of 3.5μm radius, 47μm pitch was used, while the material parameters are the same as we used in our model. Fig. 3(b) shows the displacement of the double helix under 0.42N load as an example. We convert the FEM simulations to the stress-strain diagram, shown in Fig. 3(c), which is linear and in agreement with the Cosserat curve model.

Fig. 4(a) shows the dependence of the distributed forces per unit length $f_1$ on the tensile strain in the entire allowed range of for $H_{DF}$ from Eqs. (15-16). According to our calculations $f_1$ is negative, which indicates that $\boldsymbol{f}$ is in the direction opposite to $\boldsymbol{d}_1$ with the consideration of $\boldsymbol{f} = f_1\boldsymbol{d}_1$. Since $\boldsymbol{d}_1$ is along the direction of the largest bending stiffness of the cross section in $H_{DF}$, $\boldsymbol{f}$ should be along the helix radial axis as shown in Fig. 2(b') and 2(c'). Moreover stretching double nanohelices and increasing the helix angle $\zeta$ would enhance the interaction between two strands. Given the length of a strand, we can get the whole interaction force of a double nanohelix with $\boldsymbol{f}$. Considering that the interaction force is difficult to be measured in contrast with the deformation and the loading force, our present model supplies a reliable reference for further experimental studies.

As mentioned earlier, the stretch of strands is responsible for the elongation of the double nanohelix with a straight contact line between two strands, therefore, as shown in Fig. 4(b) we study the ratio of the stretching length $\Delta L$ of nanowire to the increment of pitch $\Delta b$ of $H_{DF}$ during the loading for 0 º$\leq \zeta \leq$ 45 ºbased on Eq. (14). $\Delta L = L_0(\lambda_2-\lambda_1)$, where $\lambda_1$ and $\lambda_2$ are the stretch of $H_{IF}$ and $H_{DF}$, respectively. For all helix angles, the more the double nanohelices deform in the axial direction, the greater contribution does the stretching length $\Delta L$ make to the elongation. Although the $\Delta L/\Delta b$ decreases with increasing the helix angle $\zeta$, the smallest ratio is still above 70% without loading and it goes up to75% at the breaking point for $\zeta$=45 º. The $\Delta L/\Delta b$ of a double helix is rather large compared to a single helix, for instance, the largest ratio is only 2.2% for a $Si_3N_4$ microhelix and 18.8% for a carbon nanohelix according to our former research on the superelasticity of single helices.[36] It is quantitatively demonstrated that the stretch of strands plays a pivotal role in the whole strain region and the analytical modeling based on extensible Cosserat curve is an efficient tool to investigate the mechanical behavior of double nanohelices. In addition, Fig. 4(c) shows the diagram of torque versus tensile strain and the helix angle $\zeta$ obtained from Eq. (17), which indicates that a larger torque is required for obtaining a closer wound double nanohelix, and an increasing load can decrease the torque along the helix axis.

The tensile modulus defined as $(hNb)/A$ is an important physical quantity to describe the mechanical behavior of double nanohelices in a direct way. Fig 4(d) illustrates how the tensile modulus depends on the tensile strain for 0 º$\leq \zeta \leq$ 45 º, derived from Eq. (18). According to the changing trend of colormap, there are slight variations in the tensile modulus of a fixed $\zeta$ during the stretching process. Even for $\zeta$ = 45 º with the highest growth, the tensile modulus only increases by 1.1 times that of the unloaded state when it is broken. Thus the tensile modulus of the rope-like double nanohelices can be regarded as a constant, *i.e.*, the values without loading force. The high mechanical stability of the tensile modulus resistant to loading is helpful for engineering applications. And with increasing the helix angle the no-load tensile modulus decreases from 98GPa to 23GPa, which implies that under the same loading force and the same geometry parameters the elongation of a double nanohelix of 45 º is 4.3 times that of a straight wire. That confirms the conclusion we obtained from Fig. 3 that the double nanohelix structures are more deformable.

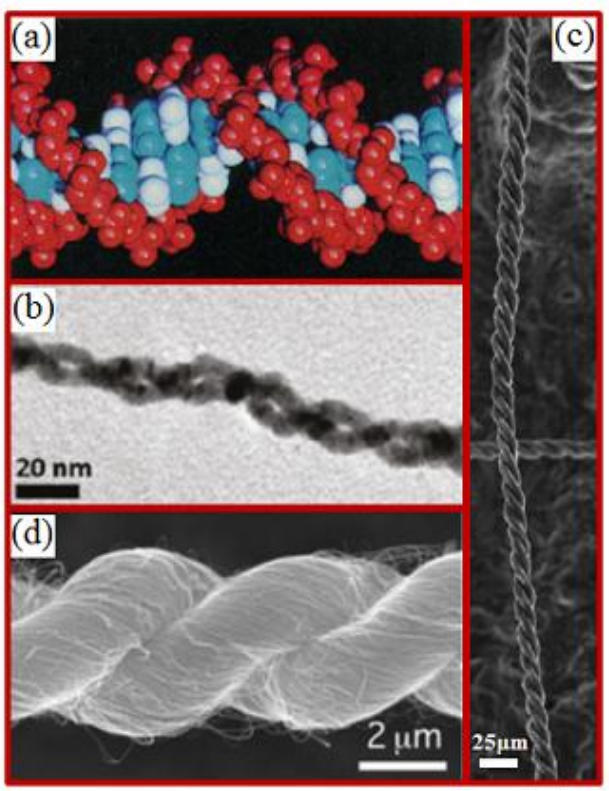


**Figure 1.** (a) Molecular modeling of DNA.[18] (b) A (Au-Ag)@Pd double nanohelix.[29] (c) A long left-handed Si double microhelix.[30] (d) A carbon double microhelix.[31] Reused with permission.[18, 29-31]

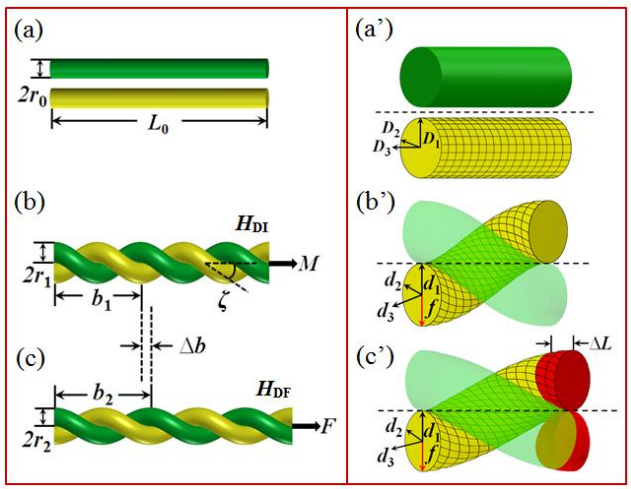


**Figure 2.** (a) Schematic illustration of two straight nanowires. (b) Configuration of the uniformly free standing double helix $H_{DI}$ under a constant torque $M$ along its helical axis. (c) Configuration of the elongated double helix $H_{DF}$ after loading by a tensile force $F$ along its helical axis. (a') A section of two straight nanowires, the corresponding sections of (b') $H_{DI}$ and (c') $H_{DF}$, respectively.

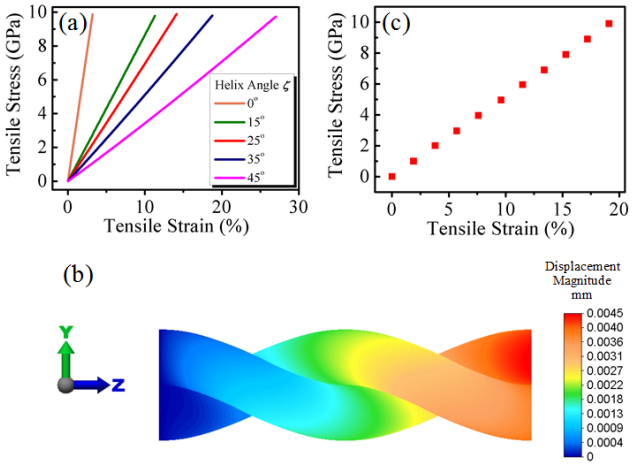


**Fig. 3.** (a) The calculations of the proposed model of tensile stress versus tensile strain during the entire stretching process for the (Au-Ag)@Pd double nanohelices with helix angle $\zeta$=0 °, 15 °, 25°, 35 °, 45 °. (b) Displacement contour plot of the FEM of a (Au-Ag)@Pd double microhelix with the helix angle $\zeta$=25° under 0.42N load. (c) The FEM simulations of tensile stress versus tensile strain.

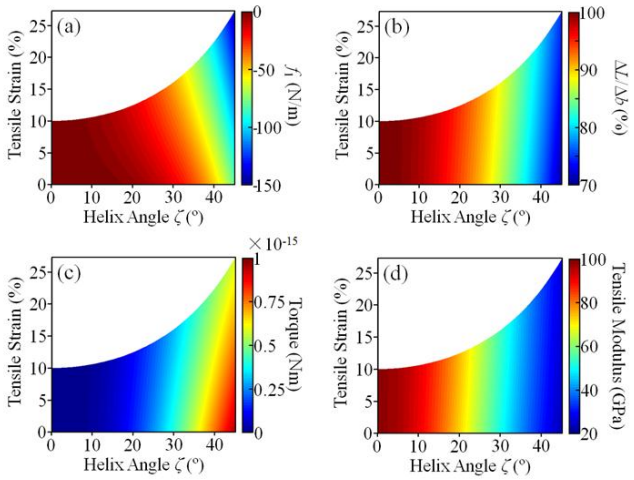


**Figure 4.** (a) Distributed forces per unit length $f_1$, (b) the ratio of the stretching length $\Delta L$ of nanowire to the increment of pitch $\Delta b$, (c) torque and (d) tensile modulus versus tensile strain and helix angle for the (Au-Ag)@Pd double nanohelices.

Cite this: DOI: 10.1039/c0xx00000x

www.rsc.org/xxxxxx

ARTICLE TYPE

**Table 1.** Structure, material and synthetic method of double helix[21-24, 26, 28-31].

| Structure | Material | Synthetic Method |
|---|---|---|
| Double helix with gaps between the two strands | Carbon | Catalytic pyrolysis of acetylene using Ni plate and powder as a catalyst[21,22] |
| | | CCVD technique using micron sized Ni as catalyst[23] |
| | | Bottom-up technique using Fe(Co)/Mg/Al LDH flake as the substrate[24] |
| | $SiO_2$ | Templated from sugar-lipid C4AG solution with different molar ratios[26] |
| Rope-like double helix | Carbon | Pyrolysis of acetone using iron nanoparticles as the catalysts[28] |
| | Au-Ag alloy | Metal (Pd, Pt, or Au) deposition on nanowires[29] |
| | Silicon | Bottom-up techniques using a Zintl compound NaSi as the starting material[30] |
| | **Materials of 1-D structure** | **Overtwisting a nanowire/nanotube/nanorod and then allowing it to relax around itself until it reached a torque-balanced state[31]** |

## Conclusions

In summary, with the aid of the extensible Cosserat curve we established an analytical model for the statics and dynamics of double helix structures, especially for those with two strands contacting along a line. By quantitatively exploring the mechanical properties of the rope-like double nanohelices with the varied helix angle, we revealed that the stretch of strands plays an important role during the loading, and wider helix angle has higher tensile stress and better elasticity. In particular, in the whole stretch regime the tensile modulus is almost constant and the elasticity of the material remains linear, which exhibits the excellent mechanical stability of the rope-like double nanohelices and is confirmed by the relevant experimental results as well as the FEM simulations. Another important result from our model is that the interaction between the strands and torque can be predicted by the derived expressions. We hope that the present study could pave the way for further experimental investigations on the mechanical properties of double nanohelices and their applications in micro- and nano-engineering.

## Acknowledgements

This work was supported by the National Natural Science Foundation of China under Grant No. 11347136, No. 11305035, and the Direct Grant for Research at The Chinese University of Hong Kong (CUHK) under the project code 4055002.

## Notes and references

[a] *School of Mathematics and Physics, Suzhou University of Science and Technology, Suzhou 215009, China*

[b] *College of Science, Donghua University, Shanghai 201620, China*

[c] *Department of Electrical and Computing Engineering, Michigan State University, United States*

[d] *Department of Mechanical and Automation Engineering, The Chinese University of Hong Kong, Hong Kong SAR, China*

*Address correspondence to L. Dai, email: dailu.1106@aliyun.com; L. Zhang, email: lizhang@mae.cuhk.edu.hk.*

**References**

1 R. Kamiya and S. Asakura, *J. Mol. Biol.*, 1976, **106**, 167.
2 R. M. Macnab and M. K. Ornston, *J. Mol. Biol.*, 1977, **112**, 1.
3 W. Helfrich, *J. Chem. Phys.*, 1986, **85**, 1085.
4 J. M. Schnur, *Science*, 1993, **262**, 1669.
5 B. Smith, Y. V. Zastavker and G. B. Benedek, *Phys. Rev. Lett.*, 2001, **87**, 278101.
6 T. McMillen and A. Goriely, *J. Nonlinear Sci.*, 2002, **12**, 241.
7 M. S. Turner, R. W. Briehl, F. A. Ferrone and R. Josephs, *Phys. Rev. Lett.*, 2003, **90**, 128103.
8 Y. Snir, and R. D. Kamien, *Science*, 2005, **307**, 1067.
9 L. Zhang, E. Ruh, D. Grtzmacher, L. X. Dong, D. J. Bell, B. J. Nelson and C. Schnenberger, *Nano Lett.*, 2006, **6**, 1311.
10 L. X. Dong, L. Zhang, D. J. Bell, D. Grützmacher and B. J. Nelson, *Journal of Physics: Conference Series*, 2007, **61**, 257.
11 K. E. Peyer, S. Tottori, F. M. Qiu, L. Zhang and B. J. Nelson, *Chemistry - A European Journal*, 2013, **19**, 28.
12 X. Q. Chen, S. L. Zhang, D. A. Dikin, W. Q. Ding, R. S. Ruoff, L. J. Pan and Y. Nakayama, *Nano Lett.*, 2003, **3**, 1299.
13 P. X. Gao, W. J. Mai and Z. L. Wang, *Nano Lett.*, 2006, **6**, 2536.
14 C. B. Cao, H. L. Du, Y. J. Xu, H. S. Zhu, T. H. Zhang and R. Yang, *Adv. Mater.*, 2008, **20**, 1738.

15 K. Hjort, J. Soderkvist and J. Schweitz, *J. Micromech. Microeng.*, 1994, **4**, 1.
16 Y. W. Hsu, S. S. Lu and P. Z. Chang, *J. Appl. Phys.*, 1999, **85**, 333.
17 G. Hwang, H. Hashimoto, D. J. Bell, L. X. Dong, B. J. Nelson and S. Schon, *Nano Lett.*, 2009, **9**, 554.
18 P. Cluzel, A. Lebrun, C. Heller, R. Lavery, J. L. Viovy, D. Chatenay, F. Caron, *Science*, 1996, **271**, 792.
19 D. S. Su, *Angew. Chem. Int. Ed.*, 2011, **50**, 4747.
20 A. S. Ivanov, A. J. Morris, K. V. Bozhenko, C. J. Pickard, and A. I. Boldyrev, *Angew. Chem. Int. Ed.*, 2012, **51**, 8330.
21 S. Motojima, M. Kawaguchi, K. Nozaki and H. Iwanaga, *Appl. Phys. Lett.*, 1990, **56**, 321.
22 S. Motojima, M. Kawaguchi, K. Nozaki and H. Iwanaga, *Carbon*, 1991, **29**, 379.
23 K. Mukhopadhyay, K. Ram, D. Lal, G. N. Mathur and K.U. Bhasker Rao, *Carbon*, 2005, **43**, 2397.
24 Q. Zhang, M. Q. Zhao, D. M. Tang, F. Li, J. Q. Huang, B. Liu, W. C. Zhu, Y. H. Zhang and F. Wei, *Angew. Chem. Int. Ed.*, 2010, **49**, 3642.
25 M. Q. Zhao, J. Q. Huang, Q. Zhang, J. Q. Nie and F. Wei, *Carbon*, 2011, **49**, 2141.
26 Y. Y. Lin, Y. Qiao, C. Gao, P. F. Tang, Y. Liu, Z. B. Li, Y. Yan and J. B. Huang, *Chem. Mater*, 2010, **22**, 6711.
27 Y. Y. Lin, A. D. Wang, Y. Qiao, C. Gao, M. Drechsler, J. P. Ye, Y. Yana and J. B. Huang, *Soft Matter*, 2010, **6**, 2031.
28 J. Liu, X. Zhang, Y. Zhang, X. Chen and J. Zhu, *Materials Research Bulletin*, 2003, **38**, 261.
29 Y. Wang, Q. Wang, H. Sun, W. Zhang, G. Chen, Y. Wang, X. Shen, Y. Han, X. Lu and H. Chen, *J. Am. Chem. Soc.*, 2011, **133**, 20060.
30 H. Morito and H. Yamane, *Angew. Chem. Int. Ed.*, 2010, **49**, 3638.
31 M. Zhang, K. R. Atkinson and R. H. Baughman, *Science*, 2004, **306**, 1358.
32 E. Cosserat and F. Cosserat, *Theorie des corps deformables*, *Hermann*, *Paris*, **1909**.
33 A. B. Whitman and C. N. DeSilva, *J. Elasticity*, 1974, **4**, 265.
34 X. Y. Ji, M. Q. Zhao, F. Wei and X. Q. Feng, *Appl. Phys. Lett.*, 2012, **100**, 263104.
35 Z. Zhou, P. Y. Lai and B. Jos, *Phys. Rev. E*, 2005, **71**, 052801.
36 L. Dai and W. Z. Shen, *Nanotechnology*, 2009, **20**, 465707.
37 J. R. Hutchinson, *J. Appl. Mech.*, 2001, **68**, 87.
38 S. Neukirch and G. H. M. Van Der Heijden, *Journal of Elasticity*, 2002, **69**, 41.
39 B. Wu, A. Heidelberg and J. J. Boland, *Nature Materials*, 2005, **4**, 525.
40 B. Wu, A. Heidelberg, J. J. Boland, J. E. Sader, X. M. Sun and Y. D. Li, *Nano Lett.*, 2006, **6**, 468.
41 S. J. Lee, S. W. Han, S.M. Hyun, H. J. Lee, J. H. Kim and Y. I. Kim, *Current Applied Physics*, 2009, **9**, S75.
42 X. Y. Qin, X. R. Zhang, G. S. Cheng and L. D. Zhang, *NanoStructured Matsrals*, 1998, **4**, 661.
43 S. U. Jen and T. C. Wu, *Thin Solid Films*, 2005, **492**, 166.
44 C. R. Barrett, W. D. Nix and A. S. Tetelman, *in The Principles of Engineering Materials Ch. 6–8, Prentice-Hall, Englewood Cliffs, New Jersey*, **1973**.